

# THE 4TH INTERNATIONAL CONFERENCE ON ALUMINUM ALLOYS

## PHYSICAL MODELLING OF MICROSTRUCTURAL EVOLUTION DURING THERMOMECHANICAL PROCESSING OF ALUMINIUM ALLOYS

E. Nes<sup>1</sup>, H.E. Vatne<sup>1</sup>, O. Daaland<sup>2</sup>, T. Furu<sup>3</sup>, R. Ørsund<sup>4</sup> and K. Marthinsen<sup>5</sup>

1. NTH, Department of Metallurgy, 7034 Trondheim, Norway

2. Hydro Aluminium A.S., R&D Center, Karmøy, Norway

3. SINTEF Materials Technology, 7034 Trondheim, Norway

4. Hydro Aluminium A.S., Research Center, Sunndalsøra, Norway

5. SINTEF Applied Physics, 7034 Trondheim, Norway

### Abstract

New physically based models for the substructure evolution, the recrystallisation kinetics, grain size and texture after single and multipass hot deformation of aluminium are presented. The approach taken differs from similar models developed for steels. The models discussed here rely on the calculation of the stored energy during deformation and the subsequent recrystallisation kinetics and related reaction products such as grain size and texture. Much effort has been directed towards identifying the nature of the nucleation sites for recrystallised grains of different crystallographic orientations. This is essential in order to elevate the model from an empirical to a physical level, the latter being necessary for a good insight into, as well as control of, the rolling process. Particle stimulated nucleation, nucleation from cube bands and grain boundary areas have been incorporated in the model. These concepts are then applied to some examples from commercial production of aluminium sheets.

### Introduction

Processing of aluminium alloys normally consists of mechanical working operations designed to effect shape changes efficiently and heat treatments for structure control to achieve desired physical and mechanical properties, important processes being forging, extrusion, hot and cold rolling. Hot rolling (or plane strain compression) is the mode of deformation discussed here, because of its commercial importance, and the scientific challenges imposed in predicting strength, grain size and texture. Industrial hot rolling is a multipass process with recrystallisation frequently taking place between the passes. The multipass aspect increases the level of complexity since one has to account for partially recrystallised regions receiving further deformation and subsequent recrystallisation. A schematic diagram of the principles of modelling the microstructural evolution in multipass hot rolling is shown in Fig. 1 (from Ref. 1). The diagram includes two types of inputs: (i) External variables, i.e. the effective strain, strain rate and temperature and (ii) internal variables, i.e. microstructural features such as volume fraction transformed, grain size, texture etc. In a structure model for rolling, the equations are used sequentially to describe the dynamic microstructural changes taking place during a pass, and the static micro-

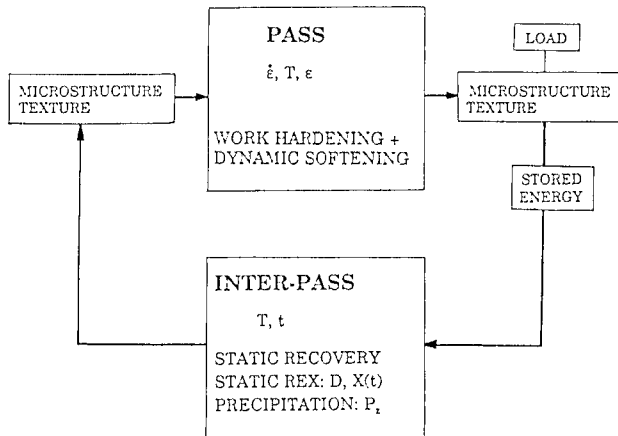


Figure 1. Schematic diagram of the principles of modelling microstructural evolution in multipass hot rolling (2).

structural changes taking place between passes, and after rolling is completed, as illustrated in Fig. 1.

While few attempts have been taken for aluminium, several modelling approaches for the development of microstructure and its effects during multipass hot rolling of steels have been reported (2-11). However, in these models a lot of empiricism has been necessary to fill the gap in physical understanding. In the present review a physically based model for the evolution of microstructure during hot rolling of aluminium is presented. The review is based on extensive micro level investigations in SEM, utilising the EBSP-technique, and in TEM, which have provided the basis for the understanding of the fundamental mechanisms for the microstructure evolution taking place (12-17). These investigations concern both nucleation and growth of recrystallised grains with an emphasis on the cube texture, due to its technological importance. This work has resulted in a preliminary model (18) predicting recrystallisation kinetics, grain size and texture after multipass hot rolling of aluminium.

The present review is based on (besides information in the general literature) the outcome of three major research programs: (i) In 1992 a Strong Point Center was established at NTH/SINTEF (Materials Departments) with the objective of developing microstructural modelling of metal processing. (ii) A French-Norwegian collaborative program (1989-93), the participating industrial partners being Pechiney and Hydro Aluminium and research partners Ecole des Mines de St.Etienne and NTH/SITNEF, and (iii) A major European Community program (1991-94) of industrial partners, Alcan International, Hydro Aluminium and Pechiney, and research partners the Materials Departments at the University of Sheffield, Manchester, NTH/SINTEF and at Risø, for details on the latter program see Ricks et al. (19) and Sellars et al. (20).

## Microstructural Modelling of Constitutive Laws for Steady State Deformation

In developing a structure model the first objective becomes to account for the roll-gap reaction, for obvious reasons. What is needed is a simple, but at the same time reasonably accurate, description of the substructure evolution in the sequential process outlined in Fig. 1. With this objective in mind we recommend the following "two-level-approach":

- (i) A global description in order to define the total stored dislocation density,  $\rho_s$ , from which the applied stress,  $\sigma$ , and stored energy,  $P_b$ , can be calculated, the latter quantity fuels the subsequent interpass softening reaction.
- (ii) A local description in order to characterize the nature and distribution of the different deformation heterogeneities. An interpass recrystallization model requires such a characterization as these heterogeneities will control the nucleation aspect.

The first of these points will be covered in this section, the second topic becomes an important element in the subsequent modelling of the interpass softening reaction.

### Background

Based on extensive investigations of the steady state conditions for creep and hot working, Sellars and Tegart (21) demonstrated that the flow stress was well represented by the following relation:

$$\sigma_s = \frac{1}{\alpha'} \operatorname{Arcsinh} \left( \frac{Z}{A'} \right)^{\frac{1}{n}} \quad (1)$$

where  $\alpha'$ ,  $A'$ ,  $n$  are temperature independent constants and  $Z$  is the Zener-Hollomon parameter,  $Z=\dot{\epsilon} \exp U/kT$ , where  $\dot{\epsilon}$  is the applied strain rate and  $U$  is an activation energy. This relationship is widely used in the modelling of metal forming processes such as hot rolling, forging and extrusion. The good fit between experimental observations and theoretical predictions is illustrated in Fig. 2, where the saturation stress for two aluminium alloys, tested in plane strain compression (22,23), are plotted as a function of  $Z$ . In calculating the  $Z$  values both Ref. 2 and 3 have used the commonly selected activation energy  $U=156000\text{J/mol}$ . It is pointed out, however, that Eq. 1 is a purely empirical relationship from which no basic physical mechanism can be inferred. This applies also to the selection of the activation energy, as a given such value defines a set of constants,  $\alpha'$ ,  $A'$  and  $n$ . To illustrate this point, consider the plane strain compression results given in Fig. 2: Although the results obtained on both the Al1Mn1Mg alloy (22) and the Al0.3Fe0.15Si alloy (23) are well represented by Eq. 1, it is not possible, based on the result from one of these alloys, to predict the behaviour of the other. Or in other words, Eq. 1 has no prediction power outside the alloy conditions tested, to which data the parameter  $U$ ,

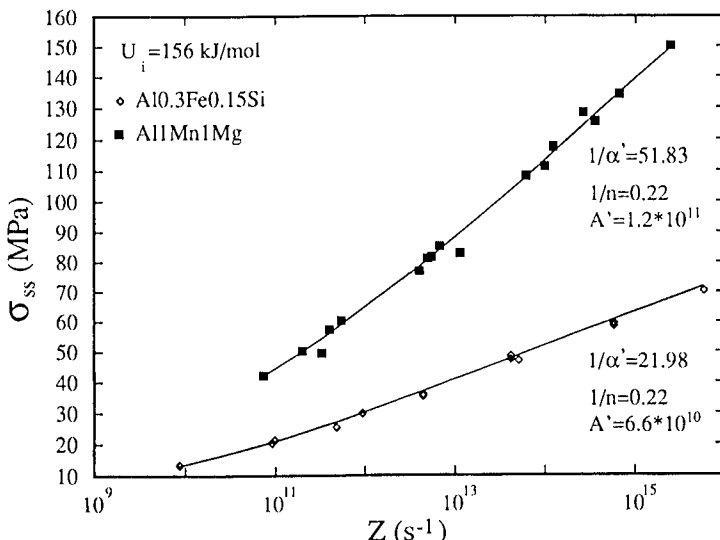


Figure 2. Steady state flow stress as a function of the Zener-Hollomon parameter for the alloys given with the activation energy fixed at 156 kJ/mol.

$\alpha'$ ,  $n$  and  $A'$  have to be fitted for each case examined. Nes (24) has in a recent work explored the possibilities for deriving an alternative, physically based relationship which is capable of correlating the steady state flow stress both to the alloy condition and the microstructural characteristics of steady state deformation. This work is briefly reviewed in the following. No attempts were made by Nes to model the "through-the-roll-gap" work hardening, only the steady state condition was treated. In handling dynamic work hardening we recommend a conventional Voce-analysis (1) in combination with the present steady-state approach.

### Model

The model developed by Nes (24) rests on the assumption that during steady state deformation of a pure metal, or stable solid solution, the substructure can be adequately described by a few microstructural elements, the two most important ones being the cell/subgrain size  $\delta$  and the dislocation density in the cell interior,  $\rho_i$ . Based on this microstructural description several possible approaches can be taken in order to calculate the flow stress, as discussed in detail in Ref. 25. Two interesting treatments being the composite theory due to Mughrabi (26,27) and Pedersen et al. (28) and a modification (25) of the original Kuhlmann-Wilsdorf (29,30) link length model. However, as shown in Ref. 25 both approaches predicts a relationship of the form

$$\tau = \tau_i + \alpha_1 G b \sqrt{\rho_i} + \alpha_2 G b \frac{1}{\delta} \quad (2)$$

where  $\tau_i$  is a frictional stress,  $G$  is the shear modulus,  $b$  is the Burgers vector and  $\alpha_1$ ,  $\alpha_2$  are constants. Based on an extensive investigation of the substructure evolution during hot deformation, Sellars and coworkers (23,31) have demonstrated that during steady state the principle of similitude applies in the sense that the separation of dislocations within the cells ( $1/\sqrt{\rho_i}$ ) scales with the cell size  $\delta$ :

$$\sqrt{\rho_i} = C_\delta / \delta \quad (3)$$

where  $C_\delta$  is a constant of typical value of the order 5. Combining this relationship with Eq. 2, it follows that the steady state flow stress can be expressed in terms of only one microstructural parameter, namely the cell/subgrain size  $\delta$ , i.e.

$$\tau = \tau_i + \alpha_3 G b \frac{1}{\delta} \quad (4)$$

where  $\alpha_3 = (C_\delta \alpha_1 + \alpha_2)$ , with  $\alpha_3$  expected to be of the order 3. In terms of the present microstructural picture the stored energy can be written:

$$P_D = \Gamma \rho_i + \kappa \gamma_{SB} \frac{1}{\delta} \quad (5)$$

where  $\Gamma = Gb^2/2$  is the dislocation line tension,  $\gamma_{SB}$  is the sub-boundary energy ( $\gamma_{SB} = \alpha_4 G b \theta (\ln e \theta_c / \theta)$  with  $\alpha_4 = 1/4\pi(1-\nu)$  and  $\theta = 3^\circ$  is the sub-boundary misorientation) and  $\kappa$  is a geometrical constant ( $\kappa=3$  for a uniform, regular substructure). Combination of Eqs. 3 and 5 gives:

$$P_D = 0.5G \left( \frac{b C_\delta}{\delta} \right)^2 + 0.05G \frac{b}{\delta} \quad (6)$$

Selecting  $C_\delta = 5$  then the second terms will totally dominate as long as  $\delta > 0.4 \mu\text{m}$ , i.e. during hot working  $P_D = 0.05Gb/\delta$  becomes a very good approximation.

The Steady State Subgrain Size. The next step is to derive an expression for the subgrain size,  $\delta$ . On the assumption that during steady state deformation the principle of similitude applies (i.e.  $\sqrt{\rho_i} = C_\delta/\delta$ ) the steady state subgrain size will be defined by the following differential equation:

$$\left[ \frac{d\delta}{dt} \right]_{\epsilon, 0K} + \left[ \frac{d\delta}{dt} \right]_{\epsilon, T} = 0 \quad (7)$$

The first, athermal, term defines the rate at which new sub-boundaries are created while the second term gives the subgrain growth rate due to dynamic recovery. An expression for the athermal,  $d\delta/dt$ -term, is obtained by reasoning as follows: If metals are deformed at room temperature one finds that the variation in the average subgrain size with strain follows a  $\delta$  vs  $\epsilon$  relationship which is of a similar type for

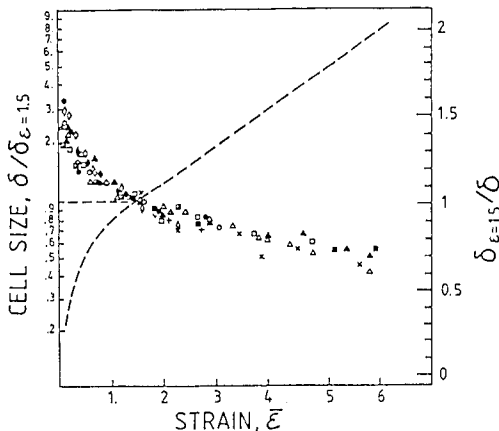


Figure 3. Subgrain/cell size as a function of equivalent strain. The size is normalized to the value found at  $\bar{\epsilon}=1.5$ . After Gil Sevillano et al (32).

a range of metals, and independent of the mode of deformation as shown in Fig. 3. (Taken from the work by Gil Sevillano et al. (32)). In Fig. 3 the variation in the inverse cell size is also given (broken line), and it can be seen that this quantity varies linearly with strain for  $\bar{\epsilon}>1$ . This is an interesting observation in view of the fact that the flow stress commonly is correlated with the inverse cell size. Accordingly, this result is consistent with a linear Stage IV work hardening behaviour. From Fig. 3 it follows that deformation at room temperature for strains  $\epsilon>\gamma M \sim 1$  gives  $1/\delta = (0.7 + 0.09\gamma)/\delta_{\epsilon=1.5}$  which in combination with Eq. 2 gives a Stage IV work hardening rate of  $\theta_{IV}^{RT} = 0.09\alpha_2Gb/\delta_{\epsilon=1.5} \sim 2 \cdot 10^{-4}G$  (for Cu,  $\delta_{\epsilon=1.5} = 0.29\mu\text{m}$  (32),  $\alpha_2 \sim 2.5$  and  $b = 2.56 \cdot 10^{-10}\text{m}$ ) which is a very reasonably RT-value indeed. As  $\theta_{IV}^{OK}/\theta_{IV}^{RT} \sim 2$  (see Gil Sevillano (33)) the  $d\delta/dt$ -term at 0K takes the form

$$\left[ \frac{d\delta}{dt} \right]_{0K} = - \frac{\theta_{IV}^{OK} \dot{\gamma} \delta^2}{\alpha_2 G_0 b} \approx - 4 \cdot 10^{-4} \frac{\dot{\gamma} \delta^2}{b} \quad (8)$$

Recovery during static annealing of deformed metals has recently been treated by Nes (25) and Furu et al. (34). These works demonstrate that static recovery can be satisfactorily treated based on an internal state variable approach comprising two variables, i.e. the cell/subgrain size and the dislocation density in the cell interior. A similar approach will be tried here in handling the dynamic case. In terms of the basic physics involved, the two types of recovery reactions (static and dynamic) are both expected to be driven by forces derived from the free energy changes associated with a reduction in the stored energy (25, 34). No attempts will be made here in accounting for the growth reactions in mechanistic terms, for such details see Refs. 25 and 34. In the following treatment of the steady state flow stress, dynamic recovery will be incorporated by assuming a situation where the sub-boundary migration is controlled by solute drag, in which case the dynamic growth rate

becomes:

$$\frac{d\delta^*}{dt} = b v_D C_B \left( \exp - \frac{U_i^b}{kT} \right) \sinh \frac{PV_a^b}{kT} \quad (9)$$

Where  $v_D$  is the Debye frequency and  $U_i^b$  is the interaction energy between the solute atom and the boundary dislocation core.  $P$  is the driving pressure for subgrain growth ( $P=2\gamma_{SB}/\delta$ , see Ref 34).  $V_a^b$  is the activation volume ( $V_a \equiv l_s^b h b$  where  $l_s^b$  is the separation of solute along the boundary dislocation line and  $h=b/\theta$  is the separation of boundary dislocation where  $\theta$  is the average sub-boundary misorientation).  $C_B$  is a constant which needs to be determined experimentally. The steady state subgrain size is now obtained by combining Eqs. 7, 8 and 9:

$$\frac{PV_a^b}{kT} > 1: \quad \frac{1}{\delta} = \frac{U_i^b}{C_1} + \frac{kT}{C_1} \ln (\dot{\epsilon} \delta^2 C_2) = \frac{kT}{C_1} \ln Z \delta^2 C_2 \quad (10)$$

$$\frac{PV_a^b}{kT} < 1: \quad \frac{1}{\delta} = \left[ \frac{kT \dot{\epsilon} C_2}{C_1} \exp \frac{U_i^b}{kT} \right]^{1/3} = \left[ \frac{kT Z C_2}{C_1} \right]^{1/3} \quad (11)$$

where  $C_1 = 2\gamma_{SB} V_a^b = 6\alpha_4 G l_s^b b^3$   $C_2 = M \cdot 10^{-4} / v_D b^2 C_B$  and  $M$  is the Taylor factor ( $\dot{\epsilon} = \dot{\gamma}/M$ ).

In aluminium alloys, the variation in subgrain size with  $T$  and  $\dot{\epsilon}$  during steady state hot deformation has been studied by several workers (22, 36, 37), the result becoming an empirical relationship of the form:

$$\frac{1}{\delta} = A \cdot \ln Z - B \quad (12)$$

where  $A^*$  and  $B^*$  are constants. The observations by Castro-Fernandez et al. (22) are plotted in Fig. 4a and the data are equally well accounted for by both Eqs. 11 and 12. In both cases an activation energy of  $U_i^b = 156\,000 \text{ J/mol}$  is used. It follows from this treatment (Eq. 10) that we have no simple substructure-Zener-Hollomon relationship. This is illustrated in Fig. 4a by solving Eq. 10 for different strain rates. It follows from Fig. 4a that within the investigated  $Z$ -range the empirical Eq. 12 gives a very good fit. However, outside this range care must be exercised in using Eq. 12. This point is well illustrated in Fig. 4b, where the subgrain size variation is plotted as a function of deformation temperature, data taken from Furu and Nes (38). The Castro-Fernandez results are also included in Fig. 4b. Note that based on these data it is not possible to draw any conclusion regarding the precise value of the activation energy. For a more detailed discussion of this important point, see Ref. 38.

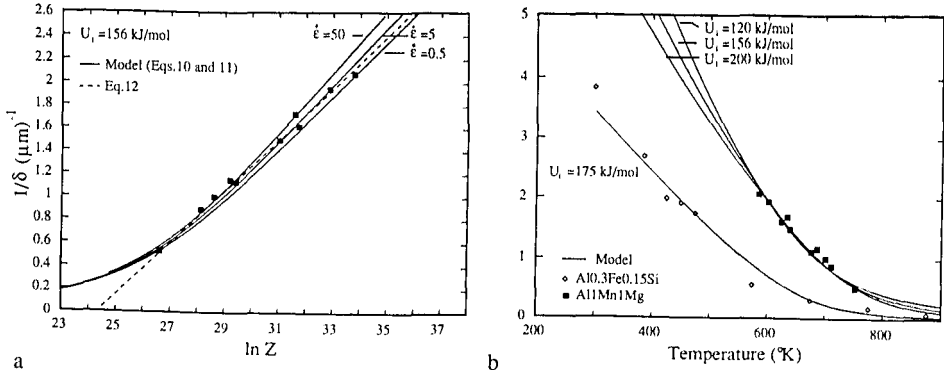


Figure 4. Dependence of subgrain size on: a) instantaneous Zener-Hollomon parameter and b) on deformation temperatures, for more details see the text.

The Steady State Flow Stress is obtained by combining Eqs. 4 and 10 which gives:

$$\sigma_s = \sigma_i + \frac{M\alpha_3 Gb}{C_1} \left[ U_i + kT \ln \frac{\dot{\epsilon}(\alpha_3 MGb)^2 C_2}{(\sigma_s - \sigma_i)^2} \right] = \sigma_i + \frac{M\alpha_3 Gb k T}{C_1} \ln \frac{Z(\alpha_3 MG)^2 C_2}{\sigma_s - \sigma_i^2} \quad (13)$$

The derivation of this equation is based on the assumption that  $PV_{\sqrt{k}}^b/kT \geq 1$  under which conditions the frictional stress  $\sigma_i$  can be treated as a constant over a considerable range in  $\dot{\epsilon}/T$  variations. This relationship can be nicely fitted to the observations of Castro-Fernandez et al. (22) as illustrated in Fig. 5. For a further analysis of the application of this model to the deformation of aluminium alloys, see Refs. 24 and 38.

### Modelling Multipass Hot Deformation

#### A Short Review of Some Existing Models.

Several models for the evolution of microstructure during hot rolling of steels have been developed over the last 10-15 years, e.g. (2-11). Typical for these models is that they rely on empirical relationships between parameters such as the time for 50% recrystallisation,  $t_{0.5}$ , and the recrystallised grain size,  $D_{rec}$ , and state variables like temperature ( $T$ ) and strain ( $\epsilon$ ) and microstructural variables such as initial grain size ( $D_0$ ) and the steel chemistry. These relationships are typically of the form

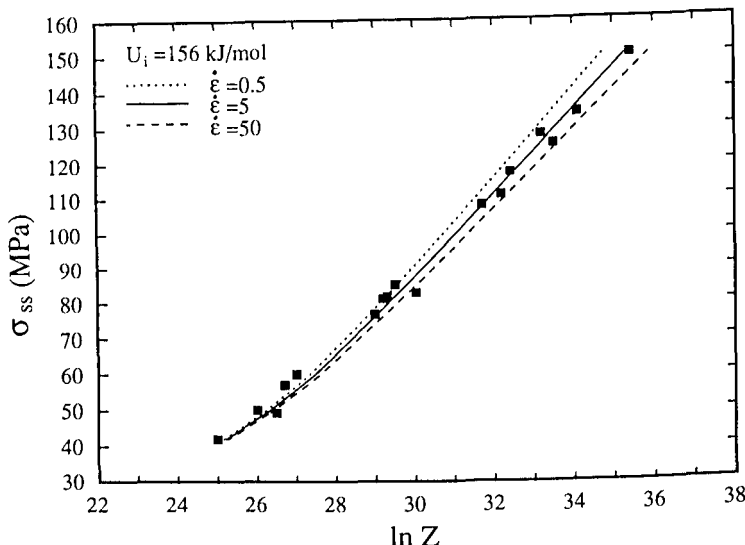


Figure 5. Steady state flow stress vs Zener-Hollomon parameter.

$$t_{0.5} = A \cdot \epsilon^{-a} \cdot D_0^b \cdot Z^{-c} \cdot \exp\left(\frac{Q_{rex}}{RT}\right) \quad (14)$$

$$D_{rex} = B \cdot D_0^d \cdot \epsilon^{-f}$$

where A, B, a, b, c, d and f are constants and  $Q_{rex}$  is the activation energy for recrystallisation. The kinetics of static recrystallisation has been assumed to be well described by an Avrami equation of the form

$$X = 1 - \exp\left[-C\left(\frac{t}{t_{0.5}}\right)^k\right] \quad (15)$$

where X is the volume fraction recrystallised after an interpass annealing time t and C and k are constants.

One obvious problem concerning these equations is the manifold of empirical tuning parameters which have to be determined specifically for each material and pre-processing history by comprehensive laboratory tests. Further, this situation is frustrating since these general equations will be able to describe about any recrystallisation process without actually revealing the important parameters and the physics behind the transformation. The danger of obtaining a good modelling result

without really understanding the process is indeed present.

Another disadvantage of these types of models is the lack of concern about the origin of the recrystallised grains. Exceptions in this connection are models which incorporate the amount of grain boundary areas where nucleation is assumed to take place (39, 40). Without the knowledge of the origin of the recrystallised grains, the models will remain at an empirical level and limit the ability to understand and control the process. The points made here emphasize the need for a better insight into the physics of the nucleation and growth reaction of the recrystallisation transformation.

The multipass aspect complicates the modelling by introducing the necessity to account for partially recrystallised regions receiving a further deformation and subsequent recrystallisation in the following passes. Two different approaches are typically reported, differing in the way of calculating the effective strain. The simplest model is to assume a single average microstructure with an effective strain  $\epsilon_{\text{eff}} = \epsilon_i + \lambda(1-X_{i,1})\epsilon_{i,1}$  where  $\lambda$  is a constant and  $X_{i,1}$  is the fraction recrystallised between the two passes of strains  $\epsilon_{i,1}$  and  $\epsilon_i$  (5,41-43). In other words, the residual strain is eliminated in the recrystallised fraction, but is unaffected in the unrecrystallised fraction, so a weighted average can simply be taken for the effective residual strain. This effective strain is taken as input in Eqs. 14 and 15 in a standard manner. The other approach as taken by the group of Sellars [2] and others [6,44] is to subdivide the partially recrystallised region according to the amount of recrystallisation and to follow each new sub-region separately for the remainder of the rolling process. The fully recrystallised volume fraction,  $X_{i,1}$ , is assumed to recrystallise independently with a strain of  $\epsilon_i$  while the unrecrystallised fraction  $1-X_{i,1}$ , is modelled using an effective strain of  $\epsilon_i + \epsilon_{i,1}$ . Clearly, several cycles of partial recrystallisation within these sub-regions result in a plethora of ever smaller zones with different microstructures. To prevent these zones becoming insignificantly small a limit of typically 5% recrystallisation is required before a new sub-region is created. Likewise, in excess of 95% recrystallisation is rounded up to 100%. This latter approach seems to have the best physical basis in the opinion of the present authors.

For aluminium alloys, the modelling is at a much earlier stage of development than for steels. Published data in the form of Eq. 14 and 15 are sparse. In those cases where such an approach has been taken, e.g. in Ref. 45, it has turned out to be difficult to describe recrystallisation during hot rolling properly by these equations. It is concluded that the simulated microstructures appear unrealistic (the main objection being a too large predicted grain size) and that some important unresolved questions in relation to modelling hot rolling of aluminium exist. This insufficiency is assumed to be due to large particles in the form of PSN (particle stimulated nucleation) speeding up the recrystallisation process or precipitates retarding the reaction through a Zener drag.

It appears that a more sophisticated and fundamental description of the microstructure evolution is required for Al-alloys than for steels. This description has to include a physical characterisation of the potential nucleation sites for

recrystallisation and their respective efficiency under various deformation conditions. An approach based on such principles has the additional advantage of predicting the texture evolution. In recent works by Furu et al.(46) and Vatne et al. (18) efforts in this direction are presented, some important elements from their treatments follow below.

### A Microstructural Model

A physical model for recrystallisation during and after hot deformation must respond in a predictable and reasonable way to deformation conditions like strain, strain rate and temperature (or Zener-Hollomon parameter Z) and material characteristics like particle size distribution, initial grain size and texture. The models by Furu et al. (46) and by Vatne et al. (18) were constructed on the basis of the following basic assumptions:

- (i) The final grain structure/texture is the result of the competition between growing grains which originate from a limited number of different types (categories) of sites where each site category has a density,  $N_i$ , and a characteristic orientation relationship to the surrounding matrix (texture component),
- (ii) near site saturation nucleation kinetics applies
- (iii) the sites are randomly distributed in space, and
- (iv) the recrystallization texture is a result of oriented nucleation.

Applying the standard assumptions (Johnson-Mehl-Avrami-Kolmogorov kinetics) of site saturation and a random distribution of nucleation sites, the following transformation kinetics law is obtained:

$$X_n(t) = 1 - \exp[-X_{ext}^n(t)] \quad (16)$$

where  $X_n(t)$  is the fraction recrystallised after the n-th pass after an inter-annealing time t and  $X_{ext}^n$  is the corresponding extended volume. The latter is determined by

$$X_{ext}^n(t) = \frac{4}{3}\pi N_{TOT}^n(G_n t)^3 \quad (17)$$

$N_{TOT}^n$  is the total number of nuclei after pass n.  $G_n$  is the growth rate of recrystallized grains, given by the expression

$$G_n = M_n (P_D^n - P_Z^n) \quad (18)$$

When  $P_D^n$  is the driving pressure due to the stored energy, defined by Eqs. 5 and 10/11,  $P_Z^n$  is the Zener drag term, and the mobility expression is of the form

$$M_n = \frac{M_0}{kT_i} \exp\left(-\frac{U_{GB}}{kT_n}\right) \quad (19)$$

where  $M_0$  is a constant,  $U_{GB}$  is the activation energy for grain boundary migration, and  $T_n$  is the temperature during the interpass annealing between the n-th and the (n+1)th pass. The mobility is assumed to be orientation independent.

Further, when the fraction recrystallised is determined the grain size in the recrystallised regions after the n-th pass,  $D_n$ , can be calculated by:

$$D_n = \left( \frac{X_n(t_n)}{N_{TOT}^n} \right)^{\frac{1}{3}} \quad (20)$$

and the volume fraction of the j-texture component,  $R_j^n$ , within the transformed material after the n-th pass is given by

$$R_j^n = N_j^n / N_{TOT}^n \quad (21)$$

The challenge now becomes to keep track of the total number of nucleation sites during the complex situation of partly recrystallised subregions. After the first pass the situation is rather simple:

$$N_{TOT}^1 = \sum_i N_i^1 \quad (22)$$

After the second rolling pass, the situation becomes more complex. Due to the partial recrystallisation with a transformed fraction  $X_1$ , the material now consists of two subregions;  $X_1$  and  $(1-X_1)$ , which must be treated separately. The number of sites after the second pass is thus given by:

$$N_{TOT}^2 = (1-X_1) \sum_i N_i^{1,2} + X_1 \sum_i N_i^2 \quad (23)$$

where  $N_i^{1,2}$  is to be understood as the density of i-sites in the material fraction which survived the first pass without recrystallising, while  $N_i^1$  are the i-sites formed during the second pass in the volume fraction which recrystallized after the first pass. The total number of nucleation sites after the n-th pass can be formulated

$$N_{TOT}^n = X_{n-1} \sum_i N_i^n + \sum_{j=0}^{n-2} X_i \left[ \prod_{k=j+1}^{n-1} (1-X_k) \right] \cdot \left[ \sum_j N_i^{j+1, \dots, n} \right] \quad (24)$$

where  $N_i^{j+1, \dots, n}$  is the number of i-sites originating from volume fractions which have survived the passes (j+1) to (n-1) without recrystallising, while  $N_i^n$  is due to i-sites that recrystallized in the pass prior to the n-th.

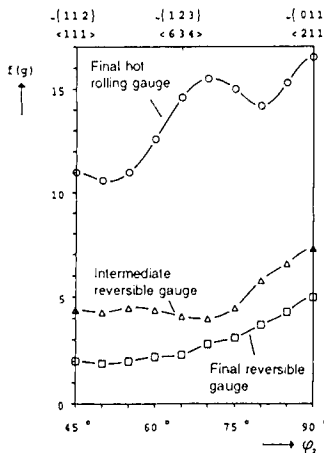


Figure 6. Maximum orientation density along the  $\beta$ -fibre versus  $\phi_2$  for samples taken at different stages of hot rolling. Al1Mn1Mg alloy, centre section of the sheet, from (12).

The problem of modelling multipass recrystallization is now reduced to: (i) rationalizing the basic assumptions listed above, (ii) identifying the salient texture components and (iii) calculating the site density  $N_i^n$ , of a given texture component after the  $n$ -th pass. This task, however, requires firstly a review of experimental observations. The experiments which will be reviewed pertains to plane strain compression of commercial purity alloys (AA 1050) and hot rolling of a commercial Al1Mn1Mg 3004 alloy.

#### The Evolution of Texture and Microstructure during Hot Rolling.

##### Hot Rolling Texture

The texture evolution during hot rolling of an Al1Mn1Mg alloy has recently been studied by Daaland (12) and Daaland and Nes (13, 14). They reported that the rolling textures after hot rolling are qualitatively similar to the textures observed after cold rolling. However, the balance between the main components of the  $\beta$ -fibre is usually different and fairly often a strong  $B_s$  component is found at the mid-thickness location of hot rolled sheets, as shown in Fig. 6. During reversible rolling, frequent recrystallization occurred in-between rolling stands, and the texture in the central layer was therefore found to resemble a mixture of rolling and annealing texture components. On the mechanisms controlling the stability of the  $B_s$  component during hot rolling see work by Hirsch (47) Hollinshead (48) and Maurice et al. (49).

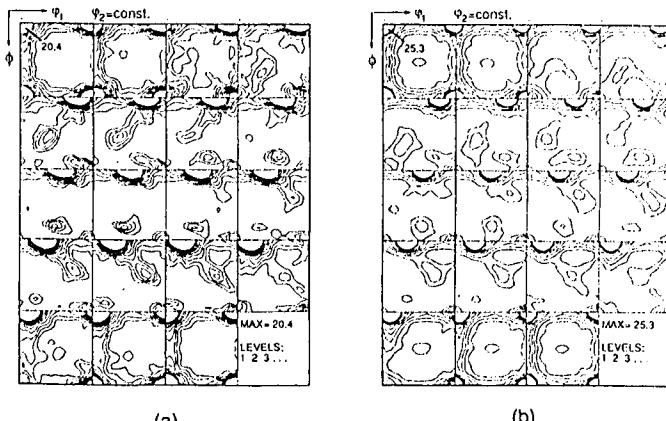


Figure 7. ODFs showing the recrystallization texture of the Al1Mn1Mg alloy after final hot rolling and subsequent annealing at 330°C. (a) surface section (b) centre section. From (12).

#### Origin of the Cube Texture Component in Hot Rolling.

The hot rolled Al1Mn1Mg alloy investigated by Daaland and Nes (12, 13) revealed a strong cube texture after annealing at exit gauge, Fig. 7. From the X-ray ODF-data the volume fraction of cube texture was estimated to ~23%. It is interesting to observe that the cube texture shows a major scattering around all the principal sample coordinates, ND, RD and TD. At a 45° RD rotation, a subsidiary peak exists corresponding to the Goss texture  $\{110\}<001>$ . In addition to cube and Goss a weak R orientation is also found as part of the recrystallization texture. Texture measurements performed on surface section-samples (Fig. 7a) shows a slightly weaker cube texture (~17%), however, the R component seems to be intensified.

The origin of the cube orientation has been a topic of much debate, investigation and speculation over a number of decades. This spectacular recrystallization texture component has been the main battle ground in the campaign between the ideas of "oriented nucleation" and "oriented growth" and strong support has been given in favour of both theories. One of the main objections to an oriented nucleation mechanism was the fact that early workers failed to find any cube orientation within the deformation texture. However, more recent electron microscope investigations have convincingly demonstrated that small volumes of cube orientation are indeed present in the as-deformed structure.

Stability of the cube orientation during hot rolling. There is substantial evidence from cold rolling experiments on cube oriented single crystals (50-52) and cube textured polycrystals (53, 54) that the cube orientation is unstable during large

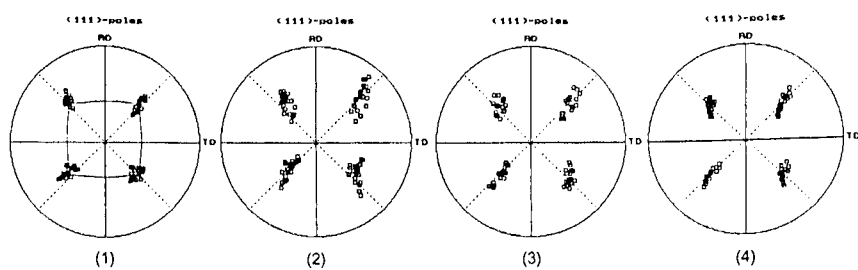
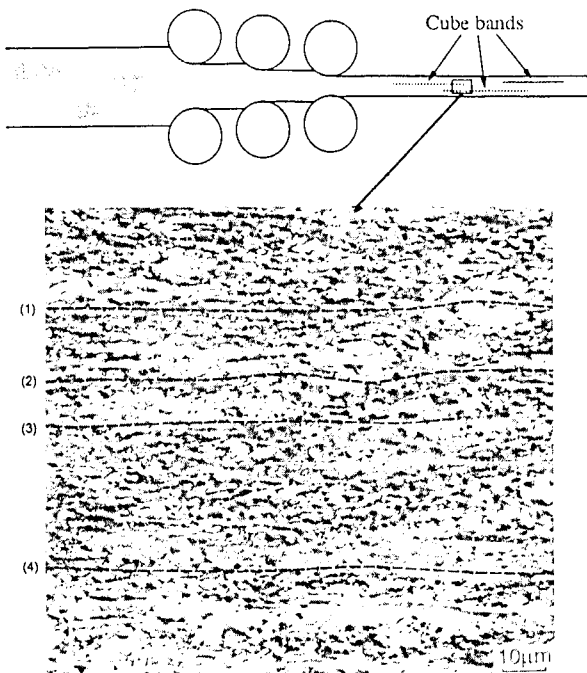


Figure 8. Channelling contrast micrograph showing the occurrence of cube oriented subgrain bands in the deformation microstructure of the Al1Mn1Mg alloy, final hot rolling gauge. (111) pole figures below the micrograph illustrates the scatter in orientations within each cube band. From (12).

rolling reductions. In the case of hot deformation of aluminium, however, increasing evidence from recent investigations (47, 55, 56) seems to suggest that the cube orientation can be relatively stable during large rolling reductions at high temperatures ( $>0.6T_m$ ). Further evidence concerning the stability of the cube texture component in hot deformation has been found in the investigation of an Al1Mn1Mg alloy by Daaland and Nes (12, 13). Using the EBSP-technique, the occurrence of the

cube orientation was investigated in samples taken at different gauges during the multipass hot rolling schedule. Investigations of samples taken after reversible rolling revealed a major portion of the cube orientation to be recrystallized grains. At the final hot rolling gauge, narrow bands or sheets of cube oriented subgrains were detected in the as-hot rolled deformation structure, extending for distances in the millimetre range along the rolling plane, Fig. 8. These cube oriented bands are separated from their neighbouring orientations by high angle boundaries and positioned in-between stable rolling texture components. Investigation of the neighbouring matrix orientations close to the cube bands showed no systematic orientation relationship. The "neighbourhoods" were generally found to consist of all possible orientations within the global orientation distribution. The lack of a gradual orientation variation across the cube band with typical divergent zones on each side of the band, therefore seems to rule out a possible transition band mechanism in the present hot rolling case. A rational and simple explanation to these observations seems to be that the cube oriented bands simply represent "old" cube grains which have survived a number of rolling passes. In other words, it seems appropriate to discuss "survival" rather than "formation" of cube during rolling.

In the context of the stability of the cube orientation some very recent observations by Akef (51) and Maurice and Driver (52) are of special interest. These authors have studied the stability of cube oriented single crystals (of pure Al and Al-Mn) during channel-die plane strain deformation at different temperatures. Their results are shown by means of (111)-pole figures in Fig. 9. During deformation at 200°C (and at room temperature) the crystal decomposes into a rather complicated set of orientations characterized by rotations of opposite sign about axes near to the TD and ND, Fig. 9a and c. The observed orientation splitting produces deformation bands separated by transition bands of the cube type, in accordance with the Dillamore and Katoh prediction. At 400°C, however, the initial cube is obviously more stable. Also during high temperature deformation a slight spread about TD is observed, but the cube orientation remains at the centre of this TD rotation up to large strains, Fig. 8b and d. These single crystal observations really support the suggestion of a metastable cube during elevated temperature deformation.

As part of the European Community funded project referred to in the introduction, the stability of cube oriented areas during deformation of an AA1050-alloy has been investigated. In order to have a controlled set of deformation conditions, specimens were plane strain compressed at Alcan International, Banbury Laboratory and Pechiney, Voreppe. Figure 10 shows the results of the investigations of the cube stability during deformation (Vatne et al. (16)). The figure is based on EBSP-scans in the normal direction in the transverse-longitudinal section. In Fig. 10a the average width of all detected cube areas is shown and b shows the line fraction of cube. Both the width and the line fraction is plotted as a function of strain for different Zener-Hollomon parameters. This EBSP-based analysis of the variation in the volume fraction of cube with increasing strain is in Fig. 10c compared to macro texture measurements for 1050 variants of various initial cube fractions as reported by Bolingbroke et al. (57). These variants were all deformed in plane strain compression at 400°C at a rate 2.5 s<sup>-1</sup>. Although the data display a certain scatter the

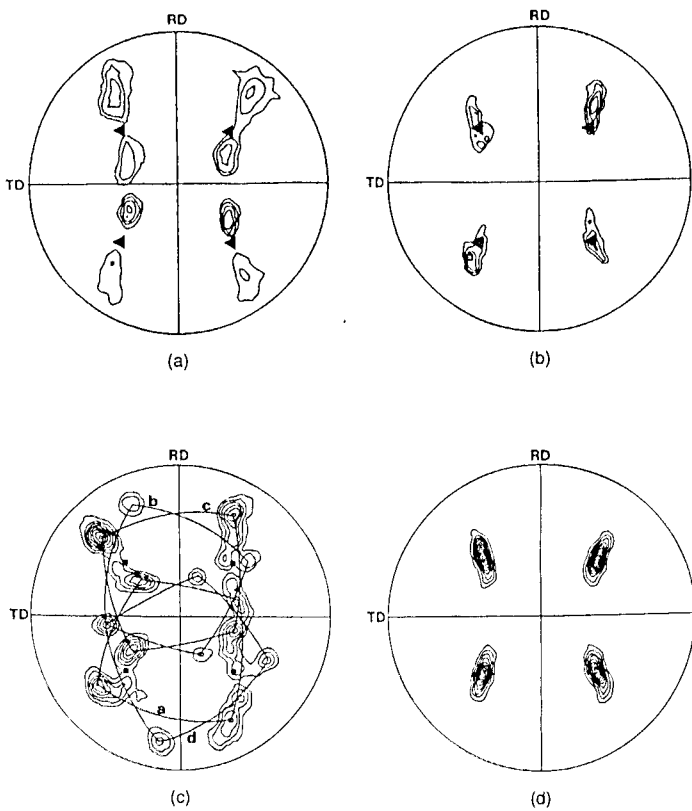


Figure 9. (111) pole figures obtained by EBSP, showing the orientation after hot channel die compression ( $\dot{\epsilon}=1.5$ ) of cube oriented single crystals; Pure Al: (a) 250°C.  $\dot{\epsilon}=10^{-2}\text{S}^{-1}$ , (b) 400°C.  $\dot{\epsilon}=10^{-2}\text{s}^{-1}$  (Akef (51)). Al-%Mg: (c) 200°C,  $\dot{\epsilon}=10^{-1}\text{s}^{-1}$ , (d) 400°C,  $\dot{\epsilon}=10^{-3}\text{s}^{-1}$  (Maurice and Driver (52)).

trend is clear, the volume fraction cube decreases with strain, dropping to about one-half at a strain of about 1.5. The data in Fig. 10c all refer to a Zener-Hollomon parameter of about  $5 \cdot 10^{12}\text{s}^1$ . Increasing the Zener-Hollomon parameter makes the cube orientation even more unstable as indicated in Fig. 10b. However, more work is required in order to quantify the strain rate and temperature effects on the stability of the cube orientation during deformation.

#### Subgrain Size Distributions and Local Variations in Stored Energy

The subgrain structure in hot rolled Al1Mn1Mg (exit gauge) has been investigated by Vatne et al. (17). In terms of the average subgrain size there seems to be no significant differences between the typical deformation texture components S, Cu, Bs

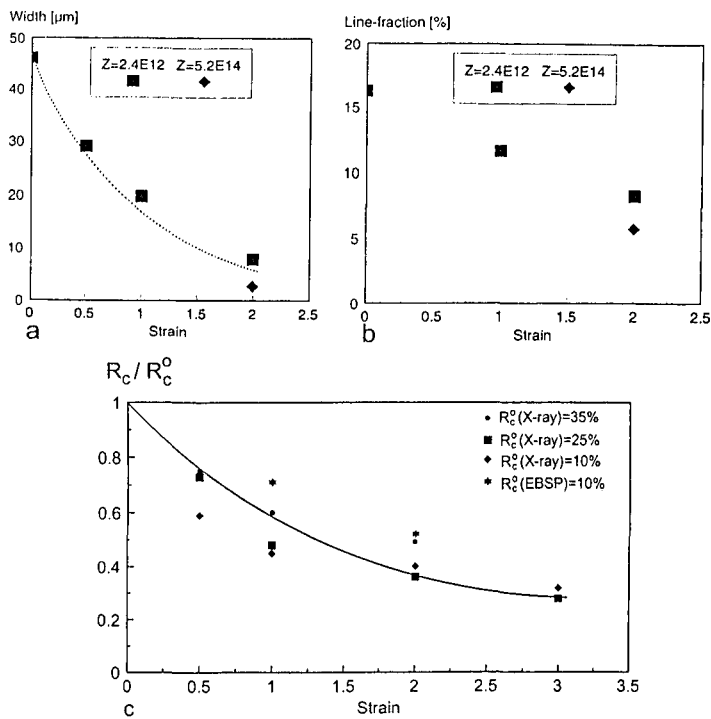


Figure 10. The effect of strain on (a) the average cube band width, (b) the cube line fraction and (c) cube volume fraction. Deformation by PSC,  $400^\circ\text{C}$ ,  $\dot{\epsilon}=2.5\text{s}^{-1}$ ,  $R_c^0 =$  initial cube volume fraction. (From Vatne et al. (16) and Bolingbroke et al. (57)).

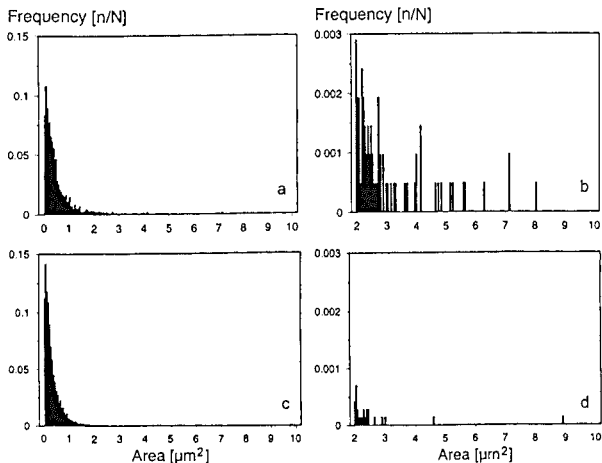


Figure 11. Subgrain size distributions: a) cubes b) tail of cubes c) other orientations, and d) tail of other orientations.

and Goss, while the average size of cube grains is significantly larger than those of the others. The most interesting difference, however, between the cube and the other subgrains pertains to the nature of the size distribution. The cube subgrain size distribution, Fig. 11, shows a long tail of extremely large subgrains which are not found in other components. Both cube subgrains and other subgrains show a log-normal distribution. A similar difference in the subgrain size distribution comparing cube oriented texture components and texture components of other orientations have been observed in a plane strain compressed 1050 alloy by Vatne et al. (16). Continued work by Vatne (unpublished) on plane strain compressed 1050 was directed towards quantifying the local variation in both subgrain size and sub-boundary misorientation, and some preliminary results are presented in Table 1. Note that the stored energy is about 30% above the average in the S-texture component, and 25% below the average in the B<sub>s</sub>-component. This may explain the reported preferential nucleation and growth from sites located in the vicinity of S-texture components (15, 16, 58) and that the B<sub>s</sub> components is the last one to be consumed during recrystallization (12,13).

Table 1. Subgrain sizes and misorientations in various texture components. Alloy 1050, plane strain compressed ( $T=400^{\circ}\text{C}$ ,  $\dot{\epsilon}=2.5$ ,  $\epsilon=2$ ).

| Components                              | S    | Cu   | Bs   | Goss | Cube | Ran.* zone | Ran.** |
|---|------|------|------|------|------|------------|--------|
| # subgrains                             | 150  | 92   | 97   | 84   | 58   | 44         | 89     |
| $\bar{\delta}[\mu\text{m}]$             | 3.84 | 4.03 | 4.41 | 3.90 | 5.48 | 4.28       | 4.11   |
| $\bar{\theta}[^{\circ}]$                | 7.78 | 6.18 | 5.35 | 6.01 | 8.57 | 20.6       | 13.3   |
| $P_D \approx \bar{\theta}/\bar{\delta}$ | 2.1  | 1.5  | 1.2  | 1.5  | 1.6  | -          | -      |
| $P_D/\bar{P}_D$                         | 1.3  | 0.9  | 0.75 | 0.9  | 1.0  | -          | -      |

\* Narrow random zones between stable texture components

\*\* Mixture of random zones and  $\beta$ -fibre components outside the main ones listed

### On the Nucleation of Cubes

As demonstrated above the widths of all observed cube areas (Fig. 10a) fall into the size range that is expected from a compression/smearing out mechanism, with a band width distribution that becomes narrower with increasing strain. Further, no signs of transition bands have been found. This means that virtually all cube areas after deformation are due to old cube grains present in the material prior to the deformation. The subgrain size measurements (Fig. 11) explains why the cube bands are so potent nucleation sites. It follows from the long tail in this distribution that some subgrains within the cube bands are overcritically large already at the as deformed stage. The reason for the large cube subgrains is unclear, but might be due to the orthogonal burgers vectors of the two most active slip systems. This unique cube geometry will facilitate annihilation of active dislocations and thus provide an

enhanced recovery rate as proposed by Ridha and Hutchinson (59). However, what is important in this context is that these large subgrains do exist. While other orientations need annealing to develop successful nuclei, the cube nuclei are already present with overcritical size in the as deformed stage. This, of course, makes cube subgrains very potent nucleation sites.

#### Other Nucleation Sites and the Origin of Random Texture

As already pointed out, the recrystallisation texture of hot rolled aluminium consists mainly of grains of cube and random orientations. There has been a consensus for many years that randomly oriented grains are due to particle stimulated nucleation (PSN). After the thorough investigations of cube bands and the nucleation from these (see above), it seems like more confidence can be put into the cube nucleation mechanism than in PSN. Also, a recent analysis by Weiland et al. (60) showed that less than about 50% of all recrystallised grains could be associated with particles and 20% with old cube grains, while the recrystallised texture contained about 75% randomly oriented grains. i.e. a significant fraction of random grains were nucleated elsewhere. Their analysis was for a cold rolled aluminium Al-Mn(Fe,Si) alloy where PSN is assumed to be especially potent due to the formation of deformation zones around large particles during cold deformation. In the case of hot rolling the deformation zones around particles are partly suppressed by recovery processes retarding the efficiency of PSN (61). Thus, a model based on PSN and cube sites exclusively, would propose extremely large grains and a cube fraction approaching 100% at high temperature deformation or a low Zener-Hollomon parameter, which is not observed experimentally. These facts give reason for questioning the PSN activity, and an additional nucleation mechanism for a random texture seems to be required for a proper description of the texture evolution. This mechanism should be activated at least at high temperatures (low Zener-Hollomon parameters), but will probably be outrun by PSN at lower temperatures. Such a mechanism has recently been proposed by some of the present authors (46), the points being as follows:

It is well known that typical textures develop during deformation, the stable (ideal) orientations being reasonably well predicted by the Taylor theory. For hot rolling of aluminium, the stable orientations belong to the Bs, S and Cu components. EBSP investigations of various hot deformed aluminium alloys (1xxx and 3xxx series) have revealed that inbetween these stable deformation texture components "thin sheets" of subgrains with random orientations are found (see Table 1). This deformation pattern seems reasonable when arguing along compatibility lines; in order to provide compatibility between stable grains of different orientations during the deformation process, more slip systems are active in the periphery of a grain (cnf. the idea of relaxed constraints). This leads to a deformation zone with large rotations and strain accumulation between the various texture components, note also the very large misorientations between subgrains (Table 1) belonging to these random zones. A speculation now becomes that these deformation zones around the old grain boundaries can act as nucleation sites for a random recrystallisation texture.

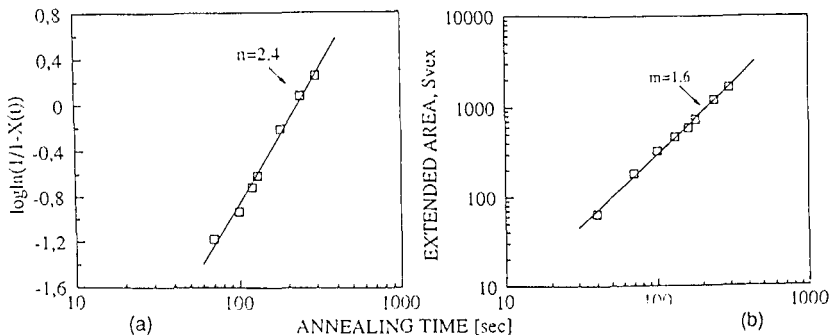


Figure 12. (a) Fraction recrystallized material as a function of annealing time and plotted in order to determine the Avrami exponent,  $n$ . (b) Plot of the extended interfacial area per unit volume as a function of annealing time. Al1Mn1Mg alloy (12).

#### Nucleation Kinetics and Growth Rate

The modelling of recrystallization requires knowledge of the nucleation kinetics. Daaland and Nes (12,14) have investigated a hot rolled Al1Mg1Mn alloy during static annealing at the exit temperature, with the result given in Fig. 12. The progress of recrystallization may be described by the familiar Avrami equation. By plotting  $\log(\ln(1/(1-X_v(t))))$  vs.  $\log t$  the Avrami-exponent can be obtained as shown in Fig. 12a, and the  $n$  value is found to equal 2.4. This value correspond to those commonly found in recrystallization but is smaller than those expected from the classical analysis. With constant growth rate in 3 dimensions  $n$  should be 3 and 4 for the site saturation and Johnson-Mehl case, respectively. By determination of the boundary area ( $S_v$ ) in addition to the volume fraction of recrystallized material ( $X_v$ ) per unit volume, it is possible to deduce the nature of the time dependence of the nucleation process, i.e. whether a site saturation or Johnson-Mehl type kinetics. This analysis is based on a Laplace transform methodology proposed by Gokhale and DeHoff (62) and further applied to recrystallization by Vandermeer and Rath (63). A stereological point counting procedure was used in order to evaluate  $S_v$ . From these data the extended interfacial area per unit volume,  $S_{vex}$ , can be calculated from the following definition (according to DeHoff (64)):

$$S_{vex} = \frac{S_v}{(1-X_v)} \quad (25)$$

A plot of  $S_{vex}$  versus annealing time now gives us a straight line with slope  $m$ , as shown in Fig. 12b. According to the above mentioned methodology the nucleation kinetics will be site saturated or time dependent (Johnson-Mehl) when the quantity  $3m-2n$  equals 0 and 1, respectively. In the Al1Mg1Mn alloy investigated here, the quantity  $3m-2n$  was found to equal 0 and it is concluded that the available nucleation

sites are activated in a time so short it may be considered to be zero relative to the total transformation time, i.e. a situation near site saturation kinetics is the most realistic.

The growth reaction was also studied in detail by Daaland and Nes (12,14), with special attention focused on comparing the growth of cube oriented grains to those belonging to other texture components. However, the possibility of an oriented growth effect was ruled out since growth rate measurements showed no higher growth rates for cube grains, although the average size of the cube grains was measured to be approximately 15% larger than those of other orientations. This size difference was attributed to other mechanism. In the 1050 alloy variants investigated by Furu et al. (46) the grain size measurements in the fully recrystallised condition showed a similar 10% difference between cube grains and grains of other orientations, i.e. a small oriented growth effect cannot be excluded but seems less likely.

### Modelling Recrystallization

The objective of the rather extensive review of experimental observations presented above was to justify the four basic assumptions (see above) on which the present model is rested. In terms the number of site categories,  $N_i$ , three such will be included in the model, i.e.  $N_{PSN}$  due to particle stimulated nucleation (PSN),  $N_c$  due to cube bands and  $N_{GB}$  which originates from the turbulent grain boundary zones. According to works by Furu et al. (46) and Vatne et al. (18) these site densities can be calculated as shown below.

In order to obtain a new grain from a potential nucleation site the following criterion (Gibbs-Thompson) has to be met; the nucleus has to reach a partially or fully high-angle character with a curvature that satisfies the following relationship:

$$R > \frac{2\gamma_{GB}}{P_D - P_z} \quad (26)$$

where  $\gamma_{GB}$  is the grain boundary energy,  $R$  is the radius of the nucleus,  $P_z$  is the Zener drag pressure and  $P_D$  is the driving pressure (stored energy) for recrystallisation, during hot deformation defined by Eqs. 4 and 10.

### Particles

Since the celebrated work by Humphreys (65, 66), particle stimulated nucleation (PSN) has been accepted as an important and often governing nucleation mechanism. The objective of the developed model is to predict the softening reactions in commercial Al-alloys containing large undefinable second phase particles. Therefore, PSN is a natural starting point. Nucleation is assumed to take place in the deformation zones that develop around large, undefinable, particles during deformation. The nuclei created in the turbulent deformation zones are assumed to have random orientations. The critical particle size for a successful nucleation event

is given by the familiar Gibbs-Thompson equation:  $\eta^* = 4\gamma_{GB}/3(P_D - P_z)$ . Following a standard calculation procedure the density of PSN sites,  $N_{PSN}$ , becomes:

$$N_{PSN} = C_{PSN} \int_{\eta^*}^{\infty} f(\eta) d\eta \quad (27)$$

where  $f(\eta)$  is the particle size distribution, and  $C_{PSN}$  is a modelling constant determining the average number of new grains generated from each particle. In aluminium alloys the large-particle-size-distribution (frequency distribution) is in general well represented by a relation of the form:  $f(\eta) = H \exp(-L\eta)$ , where  $H$  and  $L$  are characteristic distribution parameters. And it follows that Eq. 27 can be written on the form:

$$N_{PSN} = C_{PSN} N_0 \exp \left( - \frac{C_{PE}}{P_D} \right) \quad (28)$$

where  $N_0 = N/L$  and  $C_{PE}$  is a constant which needs to be determined experimentally. This latter constant includes the distribution parameter  $L$  and reflects the uncertainties in quantifying parameters like grain boundary energy and stored energy.

### Cube sites

It has been documented above that the nucleation of the cube recrystallisation texture component is associated with "old" cube grains which have survived a number of rolling passes, by which a configuration capable of regenerating new cubes has been established. The following observations summarise the basis for this nucleation mechanism:

- (i) "Old" cube oriented grains remain metastable during deformation. The cubes that survive the deformation are deformed to band-like shapes which upon annealing act as nucleation sites for new cube grains.
- (ii) Subgrains within the cube bands have a size advantage compared to subgrains of other orientations, with a typical size distribution having a long tail towards large subgrains.

The nucleation mechanism for the cube recrystallisation texture component is schematically illustrated in Fig. 13. A strain-induced-boundary-migration type of mechanism is assumed by Furu et al. (46), i.e. the boundary area of all "old" cubes are regions from which the new cubes can be nucleated.

It follows that the density of cube sites,  $N_c$ , is given by

$$N_c = \delta A(\epsilon) R_c (1 - R_c) S_c \quad (29)$$

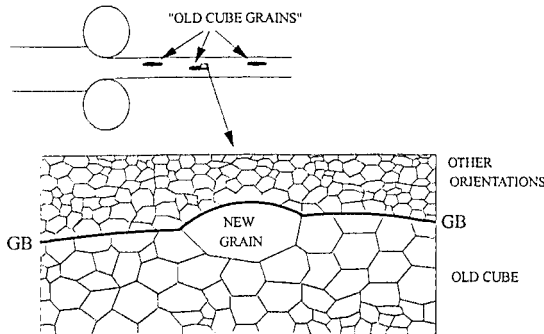


Figure 13. Nucleation of cube, schematically.

where  $\delta$  is the average subgrain size (determined by Eqs. 10 or 11,  $A(\epsilon)$  is the surface area per unit volume of cube grains of initial average size  $\bar{D}$  that have undergone a deformation of an effective strain  $\epsilon$ ,  $R_c$  is the instantaneous volume fraction of cube. Since a cube grain with another cube as neighbour cannot provide cube nuclei, only the fraction  $(1-R_c)$  is included, and  $S_c^*$  is the density of subgrains inside the cube regions with diameters larger than a critical value given by

$$\delta^* = \frac{4\gamma_{GB}}{(P_D - P_Z)} \quad (30)$$

From simple geometry it follows that

$$A(\epsilon) = 2 \frac{R_c}{\bar{D}} \exp(\epsilon) \quad (31)$$

where  $\bar{D}$  is the average size of the cube grains in the material prior to deformation.

The number of subgrains per unit volume larger than  $\delta^*$  is

$$S_c^* = \int_{\delta^*}^{\infty} f_c(\delta) d\delta \quad (32)$$

where  $f_c(\delta) = dn_c/d\delta$  is the subgrain size frequency distribution in 3D ( $dn_c$  is the number of cube subgrains per unit volume of size between  $\delta$  and  $\delta+d\delta$ ). As this distribution is properly quantified experimentally (Fig. 11), this integral can easily be solved numerically. By combining Eqs. 29-32 the density of cube sites now becomes

$$N_c = \frac{2\delta R_c(1-R_c)S_c^*}{D} \exp(\epsilon) \quad (33)$$

### Grain Boundary Sites, Randomly Oriented

As suggested by Furu et al. (46), the turbulent grain boundary zones (see above) may, in addition to the PSN-sites, contribute to the fraction of randomly oriented grains. This nucleation mechanism is based on a Bailey and Hirsch type of mechanism very analogous to the mechanism presented for the cube texture above. In analogy with Eq. 32 the density of overcritical nuclei in these random zones become

$$S_{GB}^* = \int_{\delta'}^{\infty} f_{GB}(\delta) d\delta \quad (34)$$

where  $f_{GB}(\delta)$  is the subgrain frequency distribution function in the GB-zones, and the total density of grain boundary sites is given by

$$N_{GB} = \frac{2\delta S_{GB}^*}{D} \exp(\epsilon) \quad (35)$$

### Multipass Hot Deformation

In this case of three site categories,  $N_{PSN}$ ,  $N_c$  and  $N_{GB}$ , the total number of nucleation sites after the n-th pass as defined by Eq. 24 can now be written on the form

$$N_{TOT}^n = N_{\eta}^n + X_{n-1}(N_C^n + N_{GB}^n) + \sum_{i=0}^{n-2} X_i \left[ \prod_{j=i+1}^{n-1} (1-X_j) \right] [N_C^{i+1, \dots, n} + N_{GB}^{i+1, \dots, n}] \quad (36)$$

where  $N_c^{i+1, \dots, n}$  is the number of cube sites originating from cube areas that have survived the passes (i+1) to (n-1) without recrystallising while  $N_c^n$  is due to cubes that recrystallised in the pass prior to the n-th. The expression for  $N_c^{i+1, \dots, n}$  is of the form

$$N_c^{i+1, \dots, n} = f(D_i, \sum_{j=i}^n \epsilon_j, R_c^i) \quad (37)$$

where the function f is specified in Eq. 33. Grain boundary sites are to be treated in a similar manner.

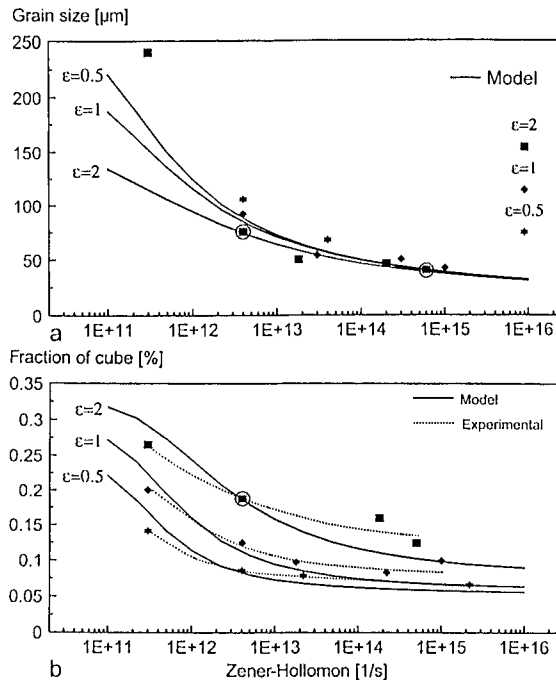


Figure 14. Recrystallized grain size (a) and volume fraction cube (b) vs the Zener-Hollomon parameter. Experimental results; deformation by PSC (Shahani (67)), for more details see (Furu et al. (46)).

#### Model Predictions

##### "Single Pass", Plane Strain Compression

A series of 1050-type alloy variants have been processed by plane strain compression at a range of different conditions by Alcan International (Bolingbroke et al. (49)) and Pechiney (Shahani (67)). The reported grain sizes and cube volume fractions are plotted as functions of the Zener-Hollomon parameter and strain in Fig. 14 and 15 respectively. The model predictions, achieved by combining Eqs. 20 and 22 with Eqs. 18, 33 and 35, are also included in Figs. 14 and 15. The modelling curves in these figures have been generated by fitting the  $\epsilon=2$ -modelling-case to the two encircled grain size observations and the cube volume fraction in Fig. 14a and b, respectively. The model then provides the shape of the  $\epsilon=2$ -curve as well as the shapes and positions of the  $\epsilon=0.5$  and  $\epsilon=1$  curves. (For more details on the model-tuning-procedure, see Furu et al. (46)). It follows from Fig. 14 that the model predictions are reasonably good, both in terms of the effect of varying  $Z$  as well as changing the

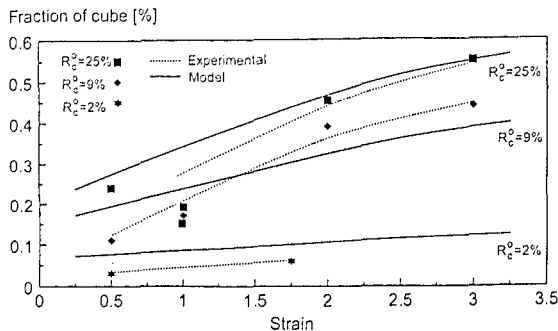


Figure 15. The effect of strain and initial cube volume fraction on the recrystallized cube texture. Experimental results (deformation by PSC, 400°C,  $\dot{\epsilon}=2.5\text{s}^{-1}$  (Bolingbroke et al. (57)) and model prediction (Furu et al. (46)).

amount of hot deformation,  $\epsilon$ . Bolingbroke et al. (57) have investigated the effect of strain on the volume fraction of cube (after subsequent recrystallization) at a constant strain rate and temperature, comparing alloys processed to give different initial volume fractions of cube oriented grains. Their results are compared to the model predictions in Fig. 15, which for strains  $\epsilon>1$  also are reasonably good.

#### Case Study: Multipass Hot Deformation of AA3004

An AA3004 alloy (can stock material) was chosen as a modelling case by Vatne et al. (18). The material was assumed to have an initial ingot grain size of 250µm and an initial cube fraction of about 5%. The particle size distribution in this type of material has been found to be well described by selecting  $N_o=1.0 \cdot 10^{16}\text{m}^{-3}$  (12) and  $L=1.3 \cdot 10^6\text{m}^{-1}$ . According to (17) the dislocation density correlates with the subgrain size as given in Eq. 6 using  $C_s=2.5$ . The mathematical basis for the present model has been outlined above. Although all equations are formulated on a physical basis, some modelling constants are unavoidable. This is partly due to uncertainties in measuring fundamental properties (like mobility, grain boundary energy, dislocation density and stored energy), uncertainties concerning the strength of the various nucleation mechanisms and the fact that some properties are material dependent.

Due to the commercial interest in hot rolling of aluminium, no company is willing to reveal any details in their pass programs. Thus, the hot rolling schedule for rolling a 600mm thick slab down to 2.5mm in 13 passes is based on reasonable guessing. The 10 first passes are performed by reversible rolling giving an increasing inter-annealing time between the passes while the 3 last passes are done on a 3-stand tandem mill resulting in very short inter-annealing times. After the last pass the material is allowed to recrystallise fully by self-annealing (for more details see Ref. 18).

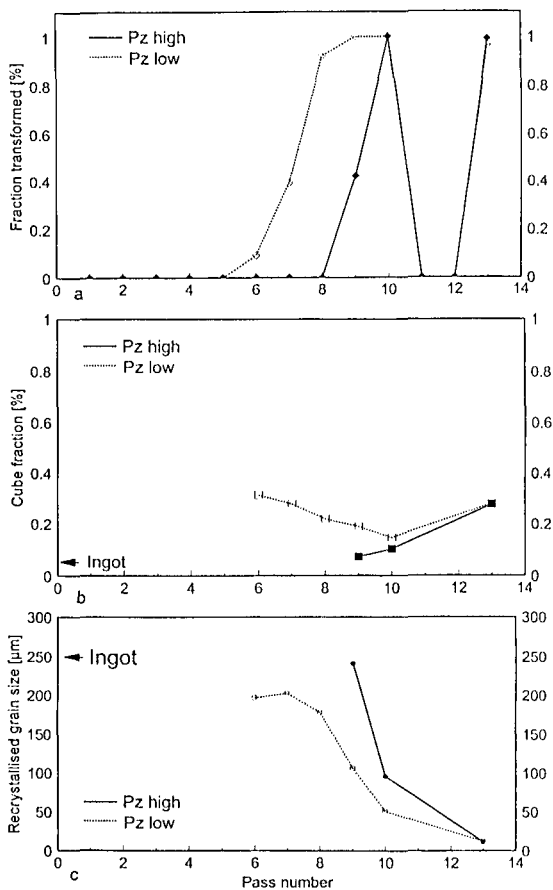


Figure 16. Hot rolling of 3004, model predictions. 13 passes with a 3-stand tandem. For more details see the text.

Precipitation during homogenization and hot rolling of 3004-type alloys will result in a high density of finely dispersed particles. Therefore, a Zener drag caused by these dispersoids was included in Eqs. 18, 26, 27 and 30. As the value of this Zener drag is difficult to determine, two cases were studied; one with a low Zener drag of the order  $P_z \sim 0.25 \cdot 10^5 \text{ J/m}^3$  and one with a higher,  $P_z \sim 0.9 \cdot 10^5 \text{ J/m}^3$ . The combination of low driving pressure and the Zener drag prevents recrystallisation during the first passes, as can be seen in Fig. 16a. In the case of a high  $P_z$  no recrystallization takes place until the 9th pass while it starts after the 6th for the low  $P_z$  case. The fraction

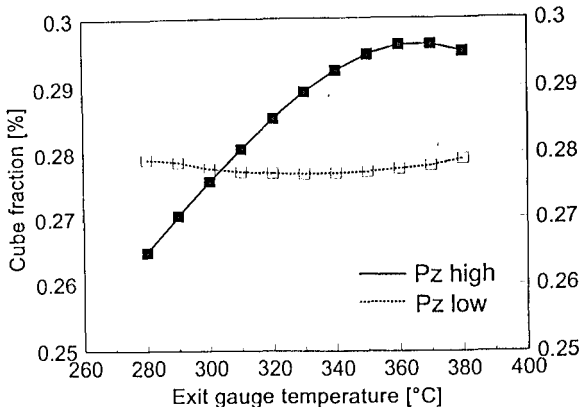


Figure 17. Volume fraction cube at the exit gauge as a function of exit temperature.

of recrystallised material increases with increasing pass number due to higher driving pressure and longer inter-annealing times. The absence of recrystallisation during the first passes allows the areas of cube surface and grain boundary regions to build up. Thus, these two nucleation mechanisms become more potent compared to PSN. This results in a relatively strong cube texture in the transformed regions at the onset of recrystallisation (6th pass). Throughout the passes the driving pressure increases. This promotes nucleation from deformation zones around particles, and the increased PSN activity causes the cube fraction to decrease. After the 10th pass (transfer gauge) the material is fully recrystallised with a cube fraction of slightly more than 10%, a value that is in good agreement with experimental observations (12,13).

Since the 3 final passes are completed in a 3-stand tandem mill, the inter-annealing times of pass 11 and 12 are so short that no recrystallisation takes place. Thus, the cube surface areas increase and the cube nucleation mechanism becomes more potent. This is further enhanced by the fact that PSN approaches its saturation limit. The result is an increase in the strength of cube and the values of almost 30% cube at the exit gauge seem reasonable. Figure 16c show that the recrystallised grain size (in the transformed material) decreases with increasing pass number. This is in accordance with the increasing driving pressure. In both cases the exit gauge recrystallised grain size was found to be slightly more than 10 $\mu$ m. The self-annealing time for fully transforming the material was in both cases of the order 1500 seconds. Both the exit grain size and the self-annealing time are in fair accordance with experimental findings. However, the values of the recrystallised grain size (~50 $\mu$ m for low  $P_z$  and ~100 $\mu$ m for high  $P_z$ ) at the transfer gauge (10th pass) are higher than experimental findings. At the transfer gauge the driving pressure is relatively low so that a Zener drag strongly influences the number of nuclei. This might indicate that the Zener drag is overestimated in the model.

Figure 17 illustrates the effect of the exit gauge temperature on the cube strength. In the low  $P_z$  case no effect is predicted. However, in the case of a high Zener drag the strength of the cube recrystallisation texture increases with increasing exit gauge temperature until it reaches a plateau and then slowly decreases. It is interesting to note that this cube behaviour is in agreement with industrial experience, as reported by Hutchinson et al. (68). It is also interesting to note that changes in the dispersoid level will, according to the present model, change the density ratios between the different types of sites (cube, particles, GB's) in a rather unforseeable way. Due to the lack of experimental data from a commercial hot-line, it is difficult to judge these model predictions. Both cases give a fair cube prediction at the transfer and exit gauges. The kinetics is best described by the high  $P_z$  case. This case also predicts the right effect of the exit gauge temperature. However, the grain size associated with the final reversible passes are too large which is an indication of that the effective driving pressure is under-estimated, for a more indepth discussion, see Vatne et al. (18).

#### Final Remarks

Although this new recrystallization model is capable of providing semi-quantitative predictions of the grain size and texture variations due to changes in the main processing variables during hot deformation, the model is at present only in an early stage of development. A more profound insight is needed into the complexities of the nucleation and growth of recrystallization before a "full-flight-model" can be constructed. On the other hand, in the opinion of the present authors, the basic physical elements have been recognized, and further, the strength of this modelling approach is that it focuses on the critical experiments required for continued progress.

#### Acknowledgements

The authors wish to thank the Research Council of Norway, NTH/SINTEF though the "Strong Point Center for Light Metals", The French-Norwegian Society, Hydro Aluminium, Pechiney and Alcan Int. for support. Thanks are also due to the European Commission for support under Contract No. BREU-CT 91-0399.

#### References

1. C.M. Sellars, The 3rd International Conference on Aluminium Alloys, ed. L. Arnberg et al., Volume 3, (Trondheim, 1992), 89.
2. C.M. Sellars and J.A. Whiteman, Met. Sci., 13, (1979), 187.
3. C.M. Sellars, Mat. Sci. Tech., 1, (1985), 352.
4. J.H. Beynon and C.M. Sellars, ISIJ International, 32 No. 3, (1992), 359.
5. P.Choquet, B. de Lamberterie, C. Perdrix and H. Biausser, Proc. of 4th Int. Steel Rolling Conf., Deauville de Recherches de la Sidérurgie, Vol. B5.1-B5.8, (1987).
6. W. Roberts, A. Sandberg, T. Siweki and T. Werlefors, "HSLA steels: technology and applications", (ed. M. Korchynsky), 67, Metals Park, OH, AMS, (1984).

7. Y. Saito, T. Enami and T. Tanaka, Trans. Iron Steel Inst. Jpn., 27, (1985), 439, 1146.
8. M. Suehiro, K. Sato, H. Yada, T. Senuma and H. Shigefuji, Y. Yamashita, Trans. Iron Steel Inst. Jpn. 27, (1987), 791.
9. E. Anelli, M. Ghersi, A. Mascanzoni, M. Paulicchi A, Aprile, F. Granato, G. Liguori and G. Rizzo, "HSLA steels: metallurgy and applications), (ed. J.M. Gray et al.), Metals Park, OH, ASM international, (1986), 693.
10. K. Esaka, J. Wakita, M. Takahashi, O. Kawano and S. Harada, Seitetsu-Kenkyu, 32, (1986), 92.
11. O. Kwon, K.B. Kang, K.J. Lee, J.K. Lee and R.W. Chand, The Structure/Property Prediction and Control Model for Plain Carbon Steels, RIST, Korea, (1988).
12. O. Daaland, PhD.thesis, The Norwegian Institute of Technology, (1993).
13. O. Daaland and E. Nes, Submitted to Acta Met. et Mater.
14. O. Daaland and E. Nes, Submitted to Acta Met. et Mater.
15. H.E. Vatne, O. Daaland and E. Nes, Material Science Forum, 157-167, 1087.
16. H.E. Vatne, R.K. Bolingbroke, E. Nes, Proceedings this Conference.
17. H.E. Vatne, S. Hofmann, A. Bardal and E. Nes, Strength of Materials., Proc. ICSMA10, The Japan Institute of Metals (1994), 255.
18. H.E. Vatne, T. Furu, R. Ørsund, K. Marthinsen and E. Nes, to be published.
19. R.A. Ricks, R.K. Bolingbroke, R.K. Shahani, R. Ørsund and G.-M. Raynaud, Proc. 15th. Risø Int. Symp. (1994).
20. C.M. Sellars, F.J. Humphreys, E. Nes and D. Juul Jensen, Proc. 15th Risø Int. Symp. (1994).
21. C.M. Sellars and W.J. McG. Tegart, Met. Rev. 17 (1972), 1.
22. F.R. Castro-Fernandez, C.M. Sellars and J.A. Whitemann, Mat. Sci and Tech., 6, (1990), 453.
23. R. Shahani, Brite Euram project, to be published.
24. E. Nes, submitted to Scripta Met.
25. E. Nes, submitted to Acta Met.
26. H. Mughrabi, in Strength of Metals and Alloys (ICSMA5) (eds. P. Haasen et al.,) Pugamon Pergamon Press, Oxford (1988), 1615.
27. H. Mughrabi, Mater. Sci. Eng., 85 (1987), 15.
28. O.B. Pedersen, L.M. Brown and W.M. Stobbs, Acta Met., 24, (1981), 1843.
29. D. Kuhlmann Wilsdorf, Met. Trans., 1 (1979), 3173.
30. D. Kuhlmann Wilsdorf, in Work Hardening in Tension and Fatigue (ed. A.W. Thompson). The Metallurgical Society of AIME, New York (1977).
31. C.M. Sellars, Materials Science Forum, 113-115, (1993), 29.
32. J. Gil Sevillano, P. Van Houtte and E. Aernoudt, Prog. Materials Sci., 25, (1980), 69.
33. J. Gil Sevillano, Plastic Deformation and Fracture of Materials (ed. H. Mughrabi), Materials Science and Technology, A Comprehensive Treatment, vol. 6, VCH, Germany, (1963).
34. T. Furu, R. Ørsund and E. Nes, Submitted to Acta Met.
35. J.P. Hirth and J. Lothe, "Theory of Dislocations", McGraw-Hill, New York (1968).
36. J.J. Jonas, C.M. Sellars and W.J. McG. Tegart, Met. Rev., 14, (1969), 1.

37. M.A. Zaidi and T. Sheppard, Metal Science, 16, (1982), 229.  
 38. T. Furu and E. Nes, Submitted to Scripta Met.  
 39. A. Yoshie, M. Fujioka, Y. Watanabe, K. Nishioka and H. Morikawa, ISIJ International, 32 No. 3, (1992), 395.  
 40. H. Yada, T. Senuma, J. Jpn. Soc. Tech. Plast., 27, (1986), 34.  
 41. P. Choquet, A. LeBon, Ch. Perdrix, "Strength of metals and alloys", Proc. of ICSMA7, (ed. H.J. McQueen et al.), Toronto, Pergamon Press, (1985), 1025.  
 42. P.D. Hodgson, R.K. Gibbs, ISIJ International, 32, No. 12, (1992), 1329.  
 43. J.E.J. Wadsworth, PhD thesis, University of Sheffield, (1989).  
 44. A. Laasraouni, J.J. Jonas, Metall. Trans. A, 22A, (1991), 151.  
 45. C.M. Sellars, Mat. Sci. Tech., 6, (1990), 6.  
 46. T. Furu, H.E. Vatne, R. Ørsund, K. Marthinsen and E. Nes, to be published.  
 47. J. Hirsch, Proc. Recrystallization' 90 (Ed. T. Chandra) TMS. Warrendale, Pa. (1990), 759.  
 48. P.A. Hollinshead, Mat. Sci. Techn., 8, (1992), 57.  
 49. C. Maurice, J. Driver and L.S. Tóth, Textures and Microstructures, 19, (1992), 211.  
 50. G.D. Köhlhoff, B. Krentsher and K. Lücke, Proc. 7th. Int. Conf. on Textures of Materials, ICOTOM7, Noordwijkerhout, Netherlands, (1984), 95.  
 51. A. Akef, PhD. Thesis, Ecole des Mines de St. Etienne, France, (1992).  
 52. C. Maurice and J. Driver, Acta Metall Mater., 41, (1993), 1653.  
 53. P.M.B. Rodrigues, H. Bickels and P. Furrer, In "Texture in Non-Ferrous Metals and Alloys", TMS, Warrendale, Pa., (1985), 45.  
 54. R.E. Sanders, S.F. Baumann and H.C. Stump, Proc. 1st. Int. Conf. on Aluminium Alloys, Charlottesville, Virginia, Voll III (1986), 1441.  
 55. P.A. Hollingshead and T. Sheppard, In "Aluminium Technology '86", The Institute of Metals, London (1986), 317.  
 56. H. Weiland and J. Hirsch, Textures and Microstructures, 14-18, (1990), 647.  
 57. R.K. Bolingbroke, G. Marshall and R. Ricks, Proceedings this Conference.  
 58. I. Samajdar and R.D. Doherty, Scripta Met, in press.  
 59. A.A. Ridha and W.B. Hutchinson, Acta Met., 30, (1982), 1929.  
 60. H. Weiland, T.N. Rouns and J. Liu, to appear in Proc., ICOTOM 10, Clausthal, (1993).  
 61. J.J. Humphreys and P.N. Kalu, Acta Met., 35, (1987), 2815.  
 62. A.M. Gokhale and R.T. DeHoff, Met. Trans., 16A, (1985), 559.  
 63. R.A. Vandermeer and B.B. Rath, Met. Trans., 20A, (1989), 391.  
 64. R.T. DeHoff, Proc. 7th. Int. Symp. on Metallurgy and Materials Science (Eds. N. Hansen et al.), Roskilde, Denmark, (1986), 35.  
 65. F.J. Humphreys, Acta Met., 25, (1977), 1323.  
 66. F.J. Humphreys, Acta Met., 27, (1979), 1801.  
 67. R. Shahani, unpublished research.  
 68. W.B. Hutchinson, A. Oscarsson and Å. Karlsson, Materials Sci. and Tech. 5, (1989), 5, 1989, 118.